

Application of Raman spectroscopy in carbon nanotube-based polymer composites

GAO Yun^{1,3}, LI LingYun^{1,4}, TAN PingHeng², LIU LuQi^{1*} & ZHANG Zhong^{1*}

¹National Center for Nanoscience and Technology of China, Beijing 100190, China;

²State Key Laboratory for Superlattices and Microstructures, Institute of Semiconductors, Chinese Academy of Sciences, Beijing 100083, China;

³Academy for Advanced Interdisciplinary Studies, Peking University, Beijing 100871, China;

⁴Graduate School of Chinese Academy of Sciences, Beijing 100190, China

Received March 6, 2010; accepted May 12, 2010

Raman spectroscopy has been widely used to identify the physical properties of carbon nanotubes (CNTs), and to assess their functionalization as well as orientation. Recently, Raman spectroscopy has become a powerful tool to characterize the interfacial properties between CNTs and polymer matrices. This review provides an overview of micro-Raman spectroscopy of CNTs and its application in studying CNT reinforced polymer composites. Based on the specific Raman band shifts relating to the mechanical deformation of CNTs, Raman scattering can be used to evaluate the interactions between the CNTs and the surrounding polymer in the composites, and to detect the phase transitions of the polymer, and investigate the local stress state as well as the Young's modulus of the CNTs. Moreover, we also review the current progress of Raman spectroscopy in various CNT macroarchitectures (such as films, fibers as well as composite fibers). The microscale structural deformation of CNT macroarchitectures and strain transfer factors from macroscale architectures to microscale structures are inferred. Based on an *in situ* Raman-tensile test, we further predict the Young's modulus of the CNT macroarchitectures and reveal the dominating factors affecting the mechanical performances of the CNT macroarchitectures.

Raman spectroscopy, carbon nanotube, composites, CNT macroarchitecture

Citation: Gao Y, Li L Y, Tan P H, et al. Application of Raman spectroscopy in carbon nanotube-based polymer composites. Chinese Sci Bull, 2010, 55: 3978–3988, doi: 10.1007/s11434-010-4100-9

Raman spectroscopy is an inelastic photon scattering spectrum, which reflects unique information concerning the vibration and electronic properties of materials. As for various types of carbon-based materials, even though these materials possess similar graphene-sheet-like microscopic structures, any minor differences existing in the structure or in the dimension could still be identified by means of Raman spectroscopy based on the different electronic properties and phonon vibrations of the materials. Raman spectroscopy, with its high sensitivity to shift-induced symmetry, its non-destructive quality, as well as its ability to be used in microanalytical studies, has become a powerful technique to

identify the microscopic structure of nanoscale carbon-based materials [1].

Recently, accompanying the deep exploration of the various properties of carbon nanotubes (CNTs), Raman spectroscopy has been widely used to investigate the structure and physical properties of CNTs. For instance, Raman spectroscopy has been employed successfully to determine the diameter and distribution of nanotubes [2–4], their metallic or semiconducting nature [5], and their orientation [6–8]. Furthermore, Raman spectra can also be used to quantify the strain or stress that the nanotubes experience under external loads [9]. Because the shifts of specific Raman bands associated with the nanotubes result from variations of the C=C bond length, it is possible to directly

*Corresponding authors (email: liulq@nanocr.cn; zhong.zhang@nanocr.cn)

evaluate the interactions between the nanotubes and polymers using Raman spectra under dynamic conditions. Here, on the basis of an overview of Raman spectroscopic studies of CNTs, recent progress of Raman measurements in CNT-based composites are reviewed.

1 Raman spectroscopy of CNTs

Carbon nanotubes (CNTs) have drawn much attention due to their unique one-dimensional structure, as well as their extraordinary electrical, mechanical and thermal properties [10]. In the past decade, scientists have focused considerable effort on investigating the structure and physical properties of CNTs [2,11–13]. Raman spectroscopy, as a non-destructive and readily available tool, has been widely used to identify CNTs, assess their diameter distribution, and to determine the structure of nanotubes [13]. Furthermore, polarized Raman spectroscopy has been used to determine the orientation of nanotubes in polymer matrices or within nanotube bundles [14–17].

1.1 Raman spectra of CNTs

Figure 1 gives a general view of the Raman spectrum expected for individual single-walled carbon nanotubes (SWNTs), revealing 4 primary features: the radial breathing mode at $160\text{--}300\text{ cm}^{-1}$, the D band at $1250\text{--}1450\text{ cm}^{-1}$, the G band at $1500\text{--}1605\text{ cm}^{-1}$ and the G' band at $2500\text{--}2700\text{ cm}^{-1}$. Each feature relates to the different vibration modes associated with the structure of CNTs.

(1) Radial breathing mode (RBM). The prominent feature in the Raman spectrum is the RBM in the $160\text{--}300\text{ cm}^{-1}$ region, associated with a symmetric movement of all of the carbon atoms in the radial direction. The frequency of the RBM is inversely proportional to the diameter of the individual nanotubes [2]. At present, the RBM is the most reliable approach to identify the structures of CNTs.

Using laser excitation wavelengths in the range from

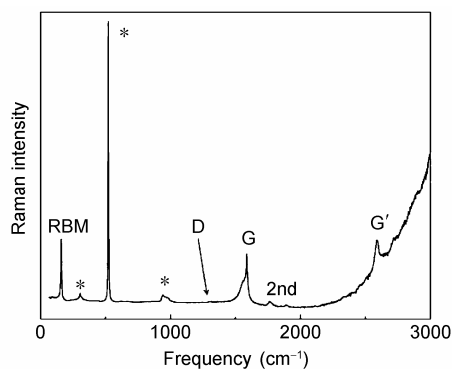


Figure 1 Raman spectrum from an individual nanotube taken over a broad frequency range using $E_{\text{laser}} = 1.58\text{ eV}$ excitation. The features marked with '*' are from the Si/SiO₂ substrate [17].

514.5 to 1320 nm, Rao and coworkers detected the Raman spectra of nanotubes (diameter from 1.2 to 1.4 nm), and investigated the dependence of Raman spectra on the laser excitation-energy. Experimental results firstly verified the uniqueness of the RBM features of SWNTs. Additionally, both the intensity and shape of the RBM features changed apparently with the variation of laser energy, owing to the one-dimensional quantum confinement of electrons in the nanotubes [18]. These results were also in good agreement with theoretical calculations based on force constants [19], as well as density functional theory [20]. Later, Jorio et al. [17] investigated the resonance Raman spectroscopy of a single SWNT deposited on a Si/SiO₂ substrate using the CVD method. They found that the diameter of a single nanotube could be derived from the frequency of its RBM feature.

The physical properties of an individual SWNT will change significantly after the formation of SWNT bundles [21]. The diameters of nanotubes within the SWNT bundles distribute over a certain range, and nanotubes with certain diameters would resonate with excited energies accordingly. According to Hulman's and Kuzmany's report [3,4], the RBM features have been successfully employed to quantitatively evaluate the diameter distribution of nanotubes in bundles. Recent work reported by Cheng's group demonstrated that the outer and inner diameters of double-walled CNTs derived from the RBM peaks of resonant Raman spectra agreed well with values determined from corresponding high resolution transmission electron microscopy images [22].

Based on the RBM Raman features, we can accurately identify the (n, m) indices of SWNTs. The determination of the (n, m) indices relies on the measurements of the diameter and electronic transition energies E_{ij} . Resonant Raman scattering measurements performed with a tunable laser provides a reliable technique to detect E_{ij} values in Raman spectra exhibiting a maximum intensity. In practice, such a tunable system has been applied to the determination of the (n, m) indices for a single nanotube. For example, the E_{ij} value of a single nanotube was measured to be $1.655 \pm 0.003\text{ eV}$, and the RBM peak appeared at 173.6 cm^{-1} . Thus, the diameter of the nanotube is 1.43 nm according to the relation $d_t = 248/173.6$, and the (n, m) indices are subsequently determined to be $(18, 0)$ [23]. Recently, Yao et al. [24] developed a novel method to construct SWNT intramolecular junctions in a controlled manner, and the corresponding (n, m) indices of the intermolecular junction were identified from the RBM features.

(2) Tangential shear mode (G). The tangential shear mode of nanotubes, namely the G band at $1500\text{--}1605\text{ cm}^{-1}$, is related to the tangential vibrations of the C atoms. The G band Raman feature consists of two main components, one peak at 1590 cm^{-1} (G^+) and another peak at $\sim 1570\text{ cm}^{-1}$ (G^-). Each component is composed of three peaks with different symmetries. The G band frequency can be used to

determine the diameter of the nanotubes, as well as distinguish between metallic and semiconducting SWNTs, and identify their orientation.

Jorio et al. [25] pointed out that the G^+ feature is independent of the nanotube diameter, whereas the G^- frequency decreases with reducing diameter. On the basis of the G^- band feature, metallic or semiconducting SWNTs could be distinguished. The G^- band feature is Lorentzian shaped for semiconducting tubes, and has a Breit-Wigner-Fano (BWF) line-shape for metallic tubes [26,27].

(3) Defect mode (D) and second order mode (G'). The D band in CNTs, appearing between 1250 and 1450 cm^{-1} , is induced by defects in the nanotubes [28]. The disorder-induced Raman band is a common feature to all sp^2 hybridized disordered carbon materials, such as graphite [29], graphite whiskers [30], graphite tubular cones [31], carbon fibers and multi-walled CNTs (MWNTs) [32]. Since the D band originates from defects, its relative intensity could reflect the degree of defects contained within the carbon materials. The greater the relative intensity, the more defects the CNTs possess [33].

Generally, the ratio of the D band to the G band (I_D/I_G) is widely used to evaluate the degree of graphitization of the CNTs and the functionalized degree of modified nanotubes through covalent bonds [34]. At the present time, Raman spectroscopy has become one of the most important tools to characterize the surface modification of nanotubes [35,36]. Simmons et al. [37] studied the effect of ozone oxidation on SWNTs. As shown in Figure 2, the ratio of I_D/I_G continued to increase with the extension of time during the ozone oxidation process, which reflects the increased functionalized

degree of the nanotubes. A similar phenomenon was also reported by Rafailov for modified nanotubes through the electrochemical approach [38]. The I_D/I_G ratio was significantly enhanced with the increase of applied voltage, indicating that a higher voltage would be beneficial to functionalize SWNTs.

The Raman G' featured at 2500–2700 cm^{-1} is the second-order overtone of the D band. Because of its strong dispersive behavior as a function of laser excitation-energy, $\Delta\omega_{G'}/\Delta E_{\text{laser}} = 106 \text{ cm}^{-1} \text{ eV}^{-1}$, many of the fundamental studies on the electronic and phonon structure of SWNTs have been done on the G' band feature [39]. In general, the D Raman feature and G' Raman feature of all sp^2 carbon materials are believed to possess similar properties [29–32, 40]. In addition, unusual two-peak structures of the G' band Raman features determined by (n, m) assignment allow us to analyze the van Hove singularities of the nanotubes [39]. Both the D mode and the G' mode have double resonance features, reflecting the interesting features of the electronic and phonon structures of the nanotubes. Since these two modes have relatively complicated scattering, much research in this area is ongoing.

1.2 Polarized Raman spectroscopy

Raman spectroscopy is an ideal characterization technique to study the orientation of CNTs. Indeed, it was observed that the intensity of the G band in the Raman spectra of oriented CNT samples decreased monotonously with an increasing angle between the nanotube axis and the polarization direction of the polarizer [41,43]. For example, Gommans et al. [6] investigated the orientation effects of nanotube bundles using polarized Raman spectroscopy. The intensity of both the G band and RBM decreased gradually when the angle between the nanotube axis and the polarizer in the region increased from 0° to 90° . Research results showed that 86% of the nanotubes were lying within a 0° to 31° region with respect to the fiber axis. Additionally, polarized Raman spectroscopy has also been used to analyze the orientation of CNTs in a polymer matrix. Bhattacharyya et al. [7] studied the crystallite orientation and the SWNT alignment in melt-blended SWNT/PP composite fibers using X-ray diffraction and polarized Raman spectroscopy, the results of which showed that the drawdown ratio of fibers during the process greatly affected the orientation effects. Hwang et al. [8] employed polarized Raman spectroscopy to demonstrate the alignment of nanotubes in a poly(methyl methacrylate) matrix.

1.3 Strain-induced Raman band shifts of CNTs

Structural deformation of a single CNT is expected to occur under an applied uniaxial strain, e.g., the elongation of bond length or decrement of force constant of $\text{C}=\text{C}$, and hence result in the downward shifts of specific Raman bands.

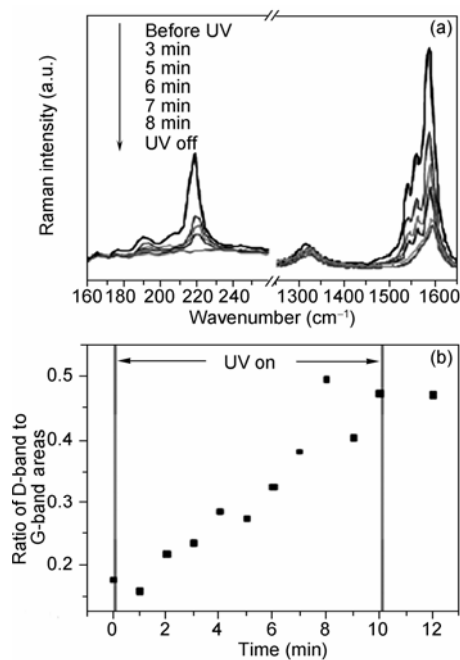


Figure 2 (a) Raman spectra of carbon nanotubes during ozone oxidation (RBM, D band and G band). (b) Ratio of I_D/I_G as a function of oxidation time.

Cronin et al. [44] strained a single SWNT using an atomic force microscopy tip as shown in Figure 3. The shift of the Raman band was recorded during the deformation process. The Raman D, G^+ , G^- and G' bands of the SWNTs shifted downwards by up to 16.1, 14.8, 12.3, 27.7 cm^{-1} under a 0.65% applied tensile strain, respectively. However, if a SWNT is broken, the Raman modes resume their original positions immediately, demonstrating the elasticity of these nanotube deformations.

The shift of the Raman bands greatly depends on the deformation modes, and it will shift upwards under a uniaxial compression, and shift downwards under tension. In reality, it is quite difficult to directly apply a uniaxial compressive strain to a single nanotube under experimental condition. An alternative method is to apply an axial compressive strain to the nanotubes through thermal shrinkage when the nanotubes are embedded in a polymer matrix. Experimental results have found out that both the Raman G and G' bands of the SWNT-based composites shifted upwards with the decrease of temperature [45].

In conclusion, the specific Raman bands of CNTs are expected to shift under deformation, and thus, Raman spectroscopy is a useful tool to investigate the interaction between CNTs and the surrounding polymer matrix. The details will be discussed in the Section 2.

2 Application of Raman spectroscopy in CNT-based composites

2.1 CNTs as a mechanical sensor in composites

In some conventional fiber-reinforced polymer composites, e.g., carbon fiber-based composites, the distribution of stress/strain fibers carried could be monitored through the shifts of the Raman bands. However, some fibers such as

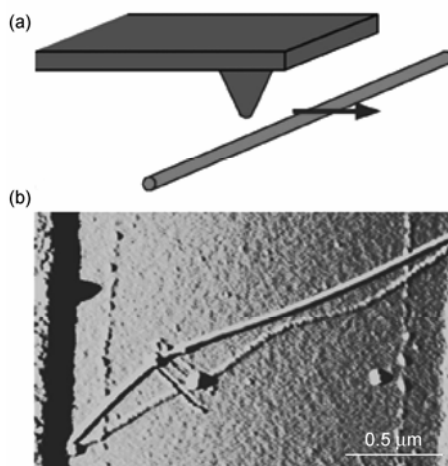


Figure 3 (a) Schematic drawing of an atomic force microscopy tip displacing a nanotube; (b) atomic force microscopy image of a metallic SWNT fixedly held at both ends by metal electrodes.

glass fibers do not have strain-sensitive Raman bands. Moreover, since most polymers (such as polycarbonate and epoxy) do not have strain-sensitive Raman bands, it is practically impossible to detect the stress/strain distributions around discontinuities in the polymers for most composites through Raman spectroscopy. Here however, after dispersing a very minor amount of CNTs inside a polymer matrix as a sensor, the stress/strain distributions of the matrix could be detected indirectly through the shifts of the CNT Raman band. As for high weight contents of CNTs incorporated in the polymer composites, nanotubes can not only act as reinforcing fillers, but they can also perform the role of mechanical sensors. Additionally, the role the interfacial properties play between the fillers and the polymer in the efficiency of stress transfer can be measured using the shift of the CNT Raman band.

(1) Monitoring the local stress distribution and interfacial interaction in conventional composites. Voids, structural defects, as well as fiber fractures, which exist in conventional fiber-reinforced polymer composites, would result in stress concentration. Zhao et al. [46] used SWNTs as a mechanical sensor to quantitatively monitor the stress-filled distribution of the SWNTs at a stress discontinuity as shown in Figure 4(a). Figure 4(b) further indicates that the experimental stress fields acquired by Raman spectroscopy fit the linear elastic solution very well.

Knowledge of the matrix stress distribution in the vicinity of the fibers in a composite material is necessary to predict its mode of failure. Zhao et al. [47] detected the distribution of the stress concentration factor in the vicinity of a broken glass fiber in a polyurethane acrylate (PUA) matrix, as captured by the randomly dispersing nanotube sensors. The contour map of the stress profile shown in Figure 5 indicates that the highest stress concentration factor occurred at the fiber break point, and this decreased gradually in both directions with increasing distance away from the break.

In general, for model fiber-based polymer composites, it is very difficult to simultaneously detect the stress distributions in the fiber and in the matrix using Raman spectroscopy

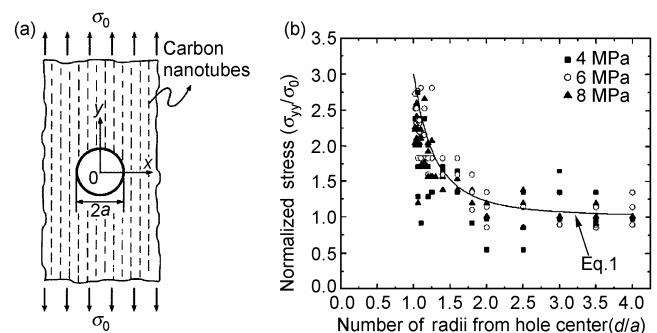


Figure 4 (a) Specimen configurations used in this study: circular hole in a thin, infinite plate under unidirectional tensile stress, including SWNTs embedded parallel to the loading axis. (b) Normalized stress along the x -axis based on the Raman G' peak shift of SWNTs, the solid line is the linear elastic solution.

owing to the strain-insensitive Raman band of most polymers. By incorporation of a small amount of SWNTs into the polymer matrix, it practically became possible to directly detect the stress transfer mechanism of a continuous high modulus carbon fiber/PUA composite. Figure 6 presents the stress distribution in a carbon fiber and in the matrix at an applied stress of 10 MPa [48]. There was a mirror image relationship between the stress distribution of the fiber between two break locations (Figure 6(a)) and the stress profile of the matrix region close to the fiber edge (Figure 6(b)). This represents the first simultaneous measurement of stress profiles in the matrix and the fiber, and the obtained results are in agreement with the classic Kelly-Tyson stress-transfer model.

Conventionally, the poor adhesion between fibers and the

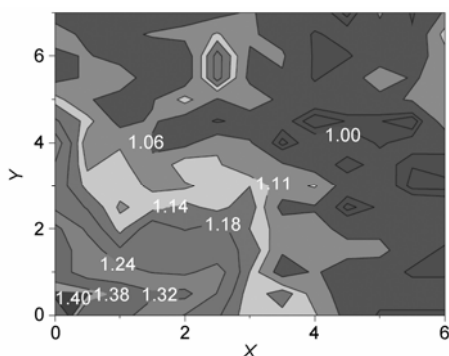


Figure 5 Two-dimensional contour map for the stress concentration factor (K_c) in the vicinity of a fiber break in an E-glass/polyurethane acrylate composite material. The break is located at the origin and only a quarter of the map is shown for simplicity. The X -axis runs along the fiber length and the Y -axis is perpendicular to the fiber length. The unit of length on both axes is the fiber radius. The highest stress concentration occurs at the point where the fiber breaks.

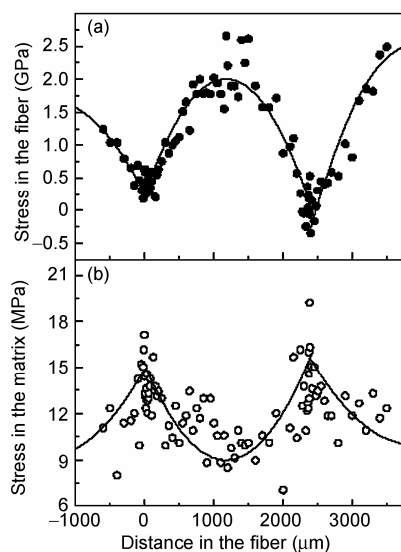


Figure 6 Stress distribution in the high modulus carbon fiber (a) and the polyurethane acrylate matrix along the fiber edge (b), measured simultaneously by Raman spectroscopy at a 10 MPa applied stress level.

polymer matrix in composites has been overcome using sizings, in which a fiber surface treated with a polymer coating (sizing) would promote adhesion behavior between the fibers and the matrix. SWNTs were employed as sensors to investigate the influence of polymer sizings with various molecular weights on the interfacial adhesion between the glass fiber and the polypropylene matrix [49]. The *in situ* Raman results showed that a better interfacial property existed when a higher modulus polymer was used as the sizings, which fitted the single fiber fragmentation test as they did before.

(2) Detection of the stress state of CNTs in composites. Since the shifts of Raman peaks are directly related to the structure deformation of CNTs, these shifts could be used to detect the reinforcing role of the nanotubes incorporated into composite materials.

Schadler et al. [50] investigated the reinforcing role of MWNTs incorporated into epoxy composites under both tension and compression modes. Mechanical results have indicated a $\sim 20\%$ improvement of the tension modulus and a $\sim 24\%$ improvement of the compression modulus obtained for composites as compared with the neat matrix. Moreover, based on the *in situ*-Raman tensile test, the Raman G' band was observed to shift upwards by $\sim 7 \text{ cm}^{-1}$ under a 1% compressive strain, whereas a slightly downward shift appeared under tension. The apparent difference between the Raman results and macroscopic mechanical results in the composites arises from the different deformation modes of the MWNTs under external loading. For instance, the outer layer of the MWNTs is expected to carry a load under tension, but it is difficult to effectively transfer the load to the inner layers due to the poor van der Waals interaction between the nanotube layers. In other words, there is no apparent deformation of the inner layers of the MWNTs under tension. Because the Raman signal is averaged over the whole of the MWNT sample, the result shows only an insignificant Raman peak shift. Unlike the tensile deformation, the load is efficiently transferred to the inner layers of the MWNTs under compression through the buckling and bending of the nanotubes. Slippage of the nanotube layers under compression is effectively prevented because of the seamless structure of the nanotubes as well as the geometrical constraint the outer layers impose on the inner layers. Therefore, obvious upward shifts of the Raman G' band under compression were observed.

Different from the shift of the Raman band of the MWNT-based composites under load, Ajayan et al. [51] found that the Raman G' band did not shift under compression and only showed a slightly downward shift under tension for SWNT-based composites. Since SWNTs tend to form bundles, slippage within the bundle would occur easily when the stress is transferred from the matrix to the nanotubes. Besides, the uniaxial tensile deformation of SWNTs is considered to be very small due to the intrinsic buckling, bending or twisting that occurs in nanotubes. Therefore,

using *in situ* Raman testing, it is hard to detect the apparent shifts of the Raman band in SWNTs under strain. Additionally, the limited spatial resolution of Raman spectroscopy must be taken into consideration, particularly since the Raman laser spot size is 1–5 μm in diameter, and the nanotubes are several nanometers in diameter. When the nanotube composites are under tension, the nanotubes lying along the tensile direction are under tension, but those aligned perpendicular to it are under compression because of the Poisson contraction. Consequently, the Raman signal is averaged over all of the nanotubes in all directions.

In the above example, the loading role of the nanotubes within the polymer is obscured greatly by the intrinsic structural features of the nanotubes, the efficiency of stress-transfer, and the distribution of the nanotubes in the polymer. Despite this, Raman shifts of $\sim 5\text{ cm}^{-1}$ under 1% tensile strain in oriented SWNT-based PUA composites were observed [52]. However, this requirement restricts the application of this method because inducing shear flow and oriented nanotubes in a polymer is not always straightforward. An alternative method is to use polarized Raman spectroscopy [47,53,54]. Significant Raman shifts were observed when the polarization direction was parallel to the nanotube axis; however, there was almost no shift when the polarization direction was perpendicular to the nanotube axis. This indicates that the reinforcing role of randomly oriented nanotubes in a polymer could be detected accurately using polarized Raman spectroscopy. Indeed, the advantage of polarized Raman spectroscopy is that the reinforcement of nanotubes in polymers is detected at the microscale, which is hard to reveal through macroscopic mechanical tests.

(3) Investigation of the influence of interfacial properties on CNT-based composites. Interfacial properties are one of the most important factors affecting the mechanical performance of various filler-based composites. As for CNT-based composites, the loading role of the nanotubes carried inside the polymer matrix, and how the interfacial adhesion between the nanotubes and the matrix behaves can be acquired simultaneously using Raman spectroscopy.

Recently, the effect of the functional groups attached to the surfaces of the nanotubes on the load-transfer efficiency was studied by Hadjiev et al. [55]. Both modified and unmodified SWNTs were employed to fabricate polystyrene composites. Raman results indicated that the efficiency of the interfacial stress-transfer of the surface modified nanotubes incorporated in the composites is higher than that of the unmodified nanotubes. Namely, the surface functional groups could improve the interfacial adhesion and allow the stress-transfer to occur more efficiently. However, the role the surface grafted groups play on the interfacial properties is still in question.

The shifts of the G band of octadecylamine (ODA) modified SWNT/epoxy composites under compression were studied [56]. The plateau of the G band appeared in the

groups appear to weaken the interfacial adhesion between the epoxy and the nanotubes. Moreover, debonding of the interfacial regions occurred with additional strain. In contrast with the situation mentioned above, the higher compressive strain was necessary to bend the nanotubes as a consequence of the strong interfacial adhesion of the unmodified nanotube-epoxy composites. The role the functional groups grafted onto the nanotube surfaces play on the interfacial adhesions were dependent on the types of functional groups, the degree of functionalization of the nanotubes, as well as the molecular structure of the polymer. Correlative work on this study is in progress.

In addition, Liu et al. [57] reported the influences of interfacial interactions on the stress-transfer capability of SWNT-OH/ Poly (vinyl alcohol) (PVA) composites. The results shown in Figure 7 indicate a linear downshift of the G' peak position under incrementally applied strain conditions within the elastic region. The varied slopes of lines fitted using the method of least squares reflected the different load-transfer capability in the composites. The larger slope of the straight line obtained for the SWNT-OH-based composites indicates the efficient stress-transfer as compared with that of the SWNT/SDS/PVA composites, which results from hydrogen bond formation between the hydroxyl groups of the modified nanotubes and the PVA itself.

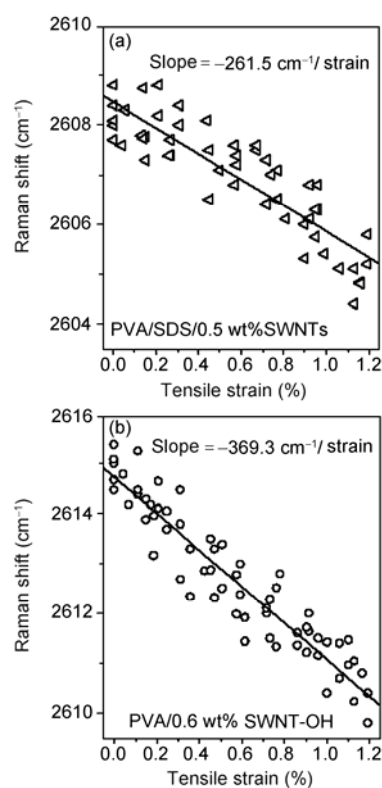


Figure 7 Plot of the Raman G' band against tensile strain applied to the PVA/SDS/0.5 wt% SWNTs (a) and PVA/0.6 wt% SWNT-OH (b) composite films.

(4) Detection of the phase transitions of polymers. The phase transitions of polymers as a function of temperature could be recorded using the dynamic mechanical testing method. Recent studies have indicated that the shifts of the G' band can also be used to detect the glass transition temperature (T_g) as well as the secondary transitions of the polymer using a SWNT-based sensor. Zhao et al. [58] observed that the G' band shifted discontinuously with variation of temperature for SWNTs embedded within amorphous bisphenol A polycarbonate and PUA composites. The upward shift of the G' band below the T_g of the polycarbonate matrix was associated with the glass-state of the polymer, in which the rigid polymer allows the efficient transfer of stress to the SWNTs. Once the temperature was above the T_g , the position of the G' band remained almost constant. In summary, the results confirmed that the SWNT-based sensor can reflect the phase transition and T_g of the polymer matrix.

2.2 Evaluation of the Young's modulus of CNTs and its composites

(1) Evaluation of the Young's modulus of CNTs. Owing to the mismatch of coefficients of thermal expansion between the polymer and the CNTs, the embedded nanotubes would be compressed gradually by the matrix with a decrease of temperature. While the G' band of the compressed nanotubes will shift upwards linearly with cooling. Because the shifts of the G' band result from the deformation of the C=C bond along the CNT-axis, Lourie et al. [59] proposed a method to evaluate the modulus of embedded individual carbon nanotubes with the help of Raman spectroscopy. The compressive strain of the nanotube along its axis is defined by eq. (1):

$$\varepsilon_{\text{nt}} = -\frac{\Delta L}{L} = \frac{\Delta \omega}{\omega}. \quad (1)$$

According to a concentric cylinder model, the axial stress of the nanotube during the cooling process is presented by eq. (2) [60]:

$$\sigma_{\text{nt}} = \frac{\Delta \alpha \Delta T}{1 + \frac{\phi_{\text{nt}}}{\phi_{\text{m}}}} E_{\text{nt}}. \quad (2)$$

Therefore, the Young's modulus of the nanotubes could be evaluated by eq. (3):

$$E_{\text{nt}} = \frac{\sigma_{\text{nt}}}{\varepsilon_{\text{nt}}}. \quad (3)$$

The resulting modulus values of the SWNTs and MWNTs are presented in Table 1. Although the values are close to the theoretical modulus, it should be pointed out that eq. (1) is a rough approximation of the compressive strain associated with CNTs.

Table 1 Young's modulus calculated from the shifts of the G' band and the theoretical values

$\Delta T(\text{K})$	$E_{\text{SWNT}} (\phi_{\text{nt}}=0.079\%)$ (GPa)	Theoretical E_{SWNT} (GPa)	$E_{\text{MWNT}} (\phi_{\text{nt}}=1.0\%)$ (GPa)	Theoretical E_{MWNT} (GPa)
-122	3577		2236	
-192	2825	5000	1718	1800
-264	3005		2437	

(2) Evaluation of the Young's modulus of SWNT macroarchitectures and their composites. Recently, much interest has been focused on the preparation of various CNT macroarchitectures (such as CNT films or fibers) and the exploration of their potential applications in many fields. [61–63] However, owing to the poor load-bearing capability, as well as the intrinsic structural defects of nanotubes, it is still a great challenge to acquire the super mechanical properties of CNTs when they are assembled into macroscale architectures. Besides, recent experimental results indicated that the mechanical properties of CNT macroarchitectures are sporadic, making systematic comparative studies difficult [61,62,64–66]. Thus, it is of fundamental importance to propose a generic methodology independent of conventional mechanical measurements to help us assess the loading role of nanotubes, and reveal the fracture mechanisms of various CNT architectures at the microscale. Lately, with the cooperation of Professor Xie's group from the Institute of Physics, Chinese Academy of Sciences, we studied the mechanical performance of SWNT macroarchitectures and their composites using *in situ* Raman spectroscopy. Based on the Raman results, we were able to predict the moduli of various CNT macroarchitectures as well as their loading capability, which were consistent with the experimental values [67,68].

CNT films were prepared using a floating catalyst chemical vapor deposition method. The resultant CNT film was formed with a reticulated structure and a high junction density between the nanotube bundles at high temperature (Figure 8(a)) [69]. Figure 8(b) shows a typical twisting procedure used to fabricate CNT fibers using a slice of as-grown CNT film as the starting material. With the help of *in situ* Raman spectroscopy, we systematically analyzed the load-bearing status of the nanotubes within the SWNT films and SWNT fibers, as well as the strain transfer efficiency, and the micro-mechanical deformation process under external loading.

(i) Strain transfer factors (STFs). To quantitatively evaluate magnitude of macroscale strain produced from the true axial strain of the CNTs inside the architectures, we defined STF (α) as the ratio of the obtained downshift rate for a strained film or fiber to the average downshift rate of the strained individual nanotubes. Based on the Raman shift rate derived from Figure 9(b), the STFs for the CNT film and fiber were calculated to be 0.017 and 0.045, respectively. Infiltrating the low-modulus and low-strength polymers, such as epoxy resin or PVA, we fabricated novel

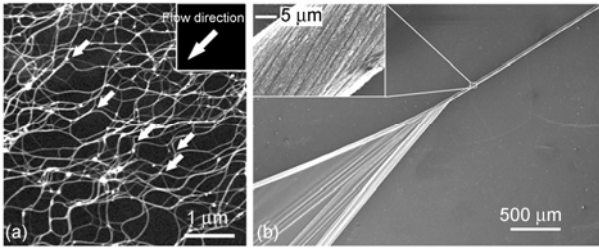


Figure 8 (a) A continuous network of nanotubes in the CNT film. (b) Scanning electron microscope image showing a piece of as-grown CNT film being twisted into a fiber.

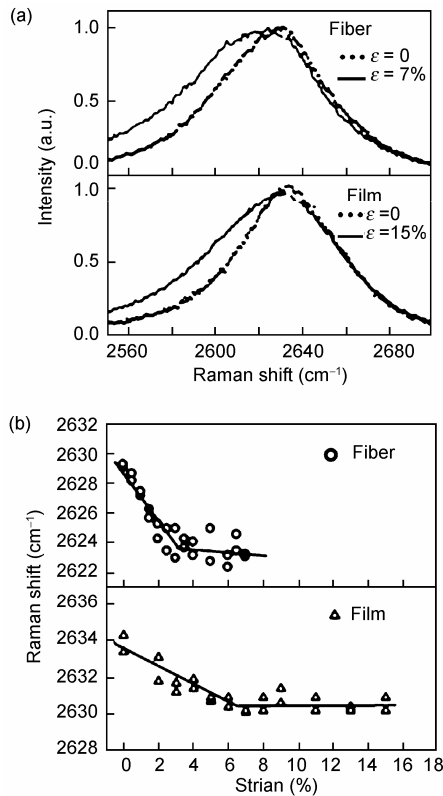


Figure 9 Typical G'-band Raman spectra of a strained CNT film and fiber. (a) Comparison of the Raman spectra for unstrained and max-strained film and fiber. (b) Raman shift of the G' band as a function of applied strain.

composite fibers with reticulated CNT architectures. Surprisingly, the STFs in the composites were enhanced remarkably by 0.4 for the epoxy composites and 0.18 for the PVA com-

posites. The elevated STFs for the reticulated CNT-based composite fibers indicate that the free deformations of the network (shown in Figure 8(a)) are effectively “frozen” by the surrounding polymer chains because of molecular level couplings, and thus the axial extension of the CNTs would increase greatly at the same macroscale strain.

(ii) Evaluation of the Young's modulus of SWNT macroarchitectures and composites. As mentioned earlier, the STFs define the axial deformation of SWNTs under a macroscale strain. After revising the classic rule of mixing, we proposed a theoretical formula to predict the modulus of SWNT macroarchitectures with STFs:

$$E = \langle \cos^2 \theta \rangle \alpha f E_t + (1 - f) E_m \quad (4)$$

where E , E_t , and E_m refer to the Young's modulus values of the architectures, the individual nanotubes, and the polymer respectively; f and α are the volume fraction of the nanotubes and STF, respectively. $\langle \cos^2 \theta \rangle$ describes the contribution of the averaged orientation angle of the nanotubes in the continuous network. For neat CNT materials, the second part of eq. (4) can be neglected.

Table 2 lists the predicted modulus values given by eq. (4) and the experimental results. From the Table, it can be seen that the revised rule of mixing fits the experimental data very well with the $\langle \cos^2 \theta \rangle$ value of 0.4–0.6, as in our macroarchitectures. Consequently, based on the Raman shift rate at the low strain region, we could predict the modulus of the SWNT macroarchitectures and its composites accurately.

Our experimental results have demonstrated that the STF is a powerful tool not only to predict the Young's modulus, but also to illuminate the key factors affecting the mechanical properties of the various SWNT macroarchitectures. In particular, STF is a complementary approach to study the macroscopic mechanical properties of SWNT-based composites.

(3) Investigation of the deformation process of SWNT macroarchitectures and composites. Besides the STF and the reinforcing role as discussed above, we could also monitor the deformation process of the SWNT architectures using the shifts of the Raman G' band at the relatively large strain. Figure 10(a) shows the shifts of the Raman G' band of various SWNT fibers as a function of the applied tensile strain. Briefly, the downward shifts versus strain curves of neat SWNT fibers and PVA/SWNT composite fibers show two-stage features, including the linear and plateau region,

Table 2 Comparison of the predicted modulus values for SWNT macroarchitectures with experimental results

Specimen	Volume fraction(f)	STF (α)	Predicted modulus (GPa)				Experimental modulus (GPa)
			$\langle \cos^2 \theta \rangle = 1/3$	$\langle \cos^2 \theta \rangle = 0.4$	$\langle \cos^2 \theta \rangle = 0.5$	$\langle \cos^2 \theta \rangle = 0.6$	
SWNT film	0.7–0.8	0.017	/	/	3.8–4.3	4.6–5.2	4–6
SWNT fiber	0.65–0.75	0.045	6–7	7–9	9–11	11–13	9–15
Epoxy/SWNT	0.3–0.4	0.4	27–36	32–43	40–53	48–63	30–50
PVA/SWNT	0.4–0.5	0.18	17–21	19–25	24–31	29–37	20–35

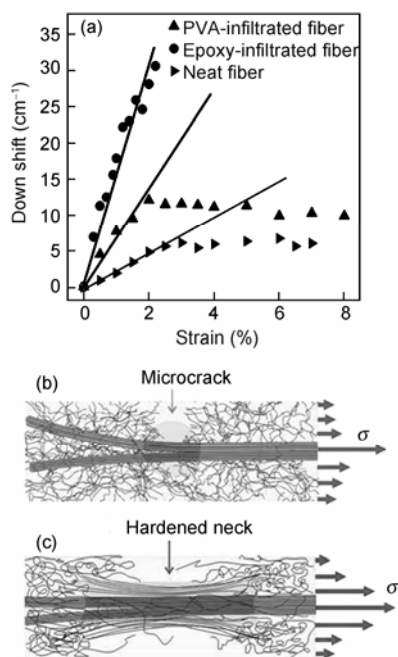


Figure 10 (a) Downward shifts of the Raman G' peak position in different systems; Schematic drawing of the fracture mechanism for (b) epoxy-infiltrated composite fiber and (c) PVA-infiltrated composite fiber.

whereas the curve of the epoxy/SWNT composite fibers show a linear trend throughout the entire strain region.

Actually, the varied shapes of the 3 downward shift-strain curves mentioned above reflect the different fracture mechanisms of the fibers. The deformation process of neat SWNT fibers under strain could be described by the following steps, in which the external loads initially distribute homogeneously within the SWNT fibers under applied strain; then the overloaded junctions start to fail and the local stress is redistributed to neighboring bundles or junctions; finally only the strongest junctions carry the loads before the breakage of the fibers. As for the epoxy/SWNT composite fibers, the chemically cross-linked 3D network of the epoxy matrix would significantly elevate the strain transfer efficiency, but it also impairs the ductility of the SWNT networks simultaneously. When micro-cracks emerge in the matrix near the junctions, the cracks propagate very fast, and the failure strains of the epoxy-infiltrated composite fibers are very close to that of the bulk epoxy resin. In contrast to the situation of epoxy-infiltrated fibers, the infiltration of PVA also restrains the structural deformation of the SWNT networks and improves the STF. Nevertheless, the orientation and stretching of linear PVA molecules could mitigate the stress concentration and protect the junctions even though interbundle slippages are widespread under large strains (Figure 10(c)). So, the failure strains of PVA-infiltrated composite fibers are not determined by that of the polymer matrix but by the extension limit of the SWNT network. When the external stress exceeds the average strength of the SWNT junctions, further added load

will no longer be homogeneously carried by all SWNT bundles but by only a part of the straight bundles that belong to strong junctions. As a result, once the strain exceeds a certain point, the peak position of the G' band plateaus until the final breakage of the specimens.

3 Conclusions

This review provides an overview of the applications of Raman spectroscopy in CNT-based polymer composites as well as the latest progress in various CNT macroarchitectures. Raman spectroscopy has been widely used to characterize the physical properties of CNTs, assess their functionalization and orientation, and to investigate their reinforcing role inside polymer matrices. The high sensitivity of the specific Raman band of the CNTs under deformation makes it possible to directly evaluate the interaction between the nanotubes and the surrounding polymer, to detect the phase transitions of the polymer, and to evaluate the Young's modulus of the CNTs. Furthermore, we have provided comments on the progress of Raman spectroscopy in various CNT macroarchitectures (such as films, fibers and its composite fibers). The deformation mechanism and the strain transfer factors of various CNT macroarchitectures are inferred, and the predicted modulus values fit the experimental results very well. All in all, microscopic mechanical analysis of CNTs using Raman spectroscopy has become a powerful and complementary approach to promote the development of CNT-based composites in many fields.

This work was supported by the National Natural Science Foundation of China (20874023, 10874177), the National Key Basic Research Program of China (2007CB936803), and the Knowledge Innovation Project of Chinese Academy of Sciences (KJX2-YW-M01).

- 1 Ferrari A C, Robertson J, ed, Tan P H, Li F, Cheng H M, translate. Raman spectroscopy in carbons: From nanotubes to diamond. Beijing: Chemical Industry Press, 2007
- 2 Dresselhaus M S, Dresselhaus G, Jorio A, et al. Raman spectroscopy on isolated single wall carbon nanotube. Carbon, 2002, 40: 2043–2061
- 3 Milnera M, Kurti J, Hulman M, et al. Periodic resonance excitation and intertube interaction from quasicontinuous distributed helicities in single-wall carbon nanotubes. Phys Rev Lett, 2000, 84: 1324–1327
- 4 Kuzmany H, Plank W, Hulman M, et al. Determination of SWCNT diameters from the Raman response of the radial breathing mode. Euro Phys J B, 2001, 22: 307–320
- 5 Tan P H, Tang Y, Hu C Y, et al. Identification of the conducting category of individual carbon nanotubes from Stokes and anti-Stokes Raman scattering. Phys Rev B, 2000, 62: 5186–5190
- 6 Gommans H H, Alldredge J W, Tashiro H, et al. Fibers of aligned single-walled carbon nanotubes: Polarized Raman spectroscopy. J Appl Phys, 88: 2509–2514
- 7 Bhattacharyya A R, Sreekkumar T V, Liu T, et al. Crystallization and orientation studies in polypropylene/single wall carbon nanotube composite. Polymer, 44: 2373–2377
- 8 Hwang J, Gommans H H, Ugawa A, et al. Polarized spectroscopy of

- aligned single-wall carbon nanotubes. *Phys Rev B*, 2000, 62: R13310–13313
- 9 Zhao Q, Wagner H D. Raman spectroscopy of carbon-nanotube-based composites. *Phil Trans R Soc Lond A*, 2004, 362: 2407–2424
- 10 Meyyappan M. *Carbon Nanotubes Science and Applications*. Boca Raton, FL: CRC Press, 2005
- 11 Collins P C, Arnold M S, Avouris P. Engineering carbon nanotubes and nanotube circuits using electrical breakdown. *Science*, 2001, 292: 706–709
- 12 Britto P J, Santhanam K S V, Rubio A. Improved charge transfer at carbon nanotube electrodes. *Adv Mater*, 1998, 11: 154–157
- 13 Dresselhaus M S, Dresselhaus G, Jorio A, et al. Monitoring oxidation of multiwalled carbon nanotubes by Raman Spectroscopy. *J Raman Spectroscopy*, 2007, 38: 728–736
- 14 Duesberg G S, Loa I, Burghard M, et al. Polarized Raman spectroscopy on isolated single-wall carbon nanotubes. *Phys Rev Lett*, 2006, 85: 5436–5439
- 15 Tartakovskii A I, Krizhanovskii D N, Kulakovskii V D. Polariton-polariton scattering in semiconductor microcavities: Distinctive features and similarities to the three-dimensional case. *Phys Rev B*, 2000, 62: 13298
- 16 Jorio A, Souza Filho A G, Brar V W, et al. Polarized resonant Raman study of isolated single-wall carbon nanotubes: Symmetry selection rules, dipolar and multipolar antenna effects. *Phys Rev B*, 2002, 65: 121402
- 17 Jorio A, Saito R, Hafner J H, et al. Structural (*n,m*) determination of isolated single-wall carbon nanotubes by resonant Raman scattering. *Phys Rev Lett*, 2001, 86: 1118–1121
- 18 Rao A M, Richter E, Shunji B, et al. Diameter selective Raman scattering from vibrational modes in carbon nanotubes. *Science*, 1997, 275: 187–191
- 19 Jishi R A, Venkataraman L, Dresselhaus M S, et al. Phonon modes in carbon nanotubes. *Chem Phys Lett*, 1993, 209: 77–82
- 20 Kurti J, Kresse G, Kuzmany H. First-principles calculations of the radial breathing mode of single-wall carbon nanotubes. *Phys Rev B*, 1999, 58: R8869–8872
- 21 Tan P H, Rozhin A G, Hasan T, et al. Photoluminescence spectroscopy of carbon nanotube bundles: Evidence for exciton energy transfer. *Phys Rev Lett*, 2007, 99: 137402
- 22 Ren W C, Li F, Chen J, et al. Morphology, diameter distribution and Raman scattering measurements of double-walled carbon nanotubes synthesized by catalytic decomposition of methane. *Chem Phys Lett*, 2002, 359: 196–202
- 23 Jorio A, Souza Filho, Dresselhaus G, et al. Joint density of electronic states for one isolated single-wall carbon nanotube studied by resonant Raman scattering. *Phys Rev B*, 2001, 63: 245416
- 24 Yao Y G, Li Q W, Zhang J, et al. Temperature-mediated growth of single-walled carbon-nanotube intramolecular junctions. *Nat Mater*, 2007, 6: 283–286
- 25 Jorio A, Pimenta M A, Dresselhaus G, et al. Resonance Raman spectra of carbon nanotubes by cross-polarized light. *Phys Rev Lett*, 2003, 90: 107403 1–4
- 26 Brown S D, Jorio A, Dresselhaus M S, et al. Observations of the D-band feature in the Raman spectra of carbon nanotubes. *Phys Rev B*, 2001, 64: 073403-073406
- 27 Jiang C, Kempa K, Zhao J, et al. Strong enhancement of the Breit-Wigner-Fano Raman line in carbon nanotube bundles caused by Plasmon band formation. *Phys Rev B*, 2002, 66: 161404–161407
- 28 Osswald S, Flahaut E, Gogotsi Y. *In situ* Raman spectroscopy study of oxidation of double- and single-wall carbon nanotubes. *Chem Mater*, 2006, 18: 1525–1533
- 29 Tan P H, Deng Y M, Zhao Q. Temperature-dependent Raman spectra and anomalous Raman phenomenon of highly oriented pyrolytic graphite. *Phys Rev B*, 1998, 58: 5435
- 30 Tan P H, Hu C Y, Dong J, et al. Polarization properties, high-order Raman spectra, and frequency asymmetry between Stokes and anti-Stokes scattering of Raman modes in a graphite whisker. *Phys Rev B*, 2001, 64: 214301
- 31 Tan P H, Zhang J, Wang X C. Raman scattering from an individual graphite tubular cone. *Carbon*, 2007, 45: 1116–1119
- 32 Tan P H, An L, Liu L Q, et al. Probing the phonon dispersion relations of graphite from the double resonance process of Stokes and anti-Stokes Raman scatterings in multi-walled carbon nanotubes. *Phys Rev B*, 2002, 66: 245410
- 33 Pimenta M A, Jorio A, Brown S D, et al. Diameter dependence of the Raman D-band in isolated single-wall carbon nanotubes. *Phys Rev B*, 2001, 64: 041401
- 34 Strano M S, Dyke C A, Usrey M L, et al. Electronic structure control of single-walled carbon nanotube functionalization. *Science*, 2003, 301: 1519–1522
- 35 Dillon A C, Gennett T, Jones K, et al. A simple and complete purification of single-walled carbon nanotube materials. *Adv Mater*, 1999, 11: 1354–1358
- 36 Zhang Y Y, Zhang J, Son H B, et al. Substrate-induced Raman frequency variation for single-walled carbon nanotubes. *J Am Chem Soc*, 2005, 127: 17156–17157
- 37 Simmons J M, Nichols B M, Baker S E, et al. Effect of ozone oxidation on single-walled carbon nanotubes. *Phys Chem B*, 2006, 110: 7113–7118
- 38 Rafailov P M, Thomsen C, Monev M, et al. Electrochemical functionalization of SWNT bundles in acid and salt media as observed by Raman and X-ray photoelectron spectroscopy. *Phys Stat Soli*, 2008, 245: 1967–1970
- 39 Dresselhaus M S, Dresselhaus G, Saito R, et al. Raman spectroscopy of carbon nanotubes. *Phys Rep*, 2005, 409: 47–99
- 40 Tan P H, Tang Y, Deng Y M, et al. Resonantly enhanced Raman scattering and high-order Raman spectra of single-walled carbon nanotubes. *Appl Phys Lett*, 1999, 75: 1524
- 41 Philippe P, Brigitte V, Pascale L. Films and fibers of oriented single wall nanotubes. *Carbon*, 2002, 40: 1741–1749
- 42 Ren W C, Li F, Cheng H M. Polarized Raman analysis of aligned double-walled carbon nanotubes. *Phys Rev B*, 2005, 71: 115428
- 43 Ren W C, Li F, Cheng H M. Aligned double-walled carbon nanotube long ropes with a narrow diameter distribution. *J Phys Chem B*, 2005, 109: 7169–7173
- 44 Cronin S B, Swan A K, Unlu M S, et al. Resonant Raman spectroscopy of individual metallic and semiconducting single-wall carbon nanotubes under uniaxial strain. *Phys Rev B*, 2005, 72: 035425
- 45 Hadjiev V G, Iliev M N, Arepalli S, et al. Raman scattering test of single-wall carbon nanotube composites. *Applied Phys Lett*, 2001, 78: 3193–3195
- 46 Zhao Q, Wood J R, Wagner H D. Stress fields around defects and fibers in a polymer using carbon nanotubes as sensors. *Appl Phys Lett*, 2001, 78: 1748–1750
- 47 Zhao Q, Wagner H D. Two-dimensional stress field mapping of fiber reinforced polymer composites using carbon nanotubes strain sensors. *Compos A*, 2003, 34: 1219–1225
- 48 Zhao Q, Frogley M D, Wagner H D. Direction-sensitive stress measurements with carbon nanotube sensors. *Poly Adv Tech*, 2001, 13: 759–764
- 49 Barber A H, Zhao Q, Wagner H D, et al. Characterization of E-glass-polypropylene interfaces using carbon nanotubes as strain sensors. *Compos Sci and Tech*, 2004, 64: 1915–1919
- 50 Schadler L S, Giannaris S C, Ajayan P M. Load transfer in carbon nanotube epoxy composites. *Appl Phys Lett*, 1998, 73: 3842–3844
- 51 Ajayan P M, Schadler L S, Giannaris C, et al. Single-walled carbon nanotube-polymer composites: Strength and weakness. *Adv Mater*, 2000, 12: 750–753
- 52 Cooper C A, Young R J, Halsall M. Investigation into the deformation of carbon nanotubes and their composites through the use of Raman spectroscopy. *Composites A*, 2001, 32: 401–411
- 53 Zhao Q, Frogley M D, Wagner H D. The use of carbon nanotubes to sense matrix stresses around a single glass fiber. *Compos Sci Tech*, 2001, 61: 2139–2143
- 54 Frogley M D, Zhao Q, Wagner H D. Polarized resonance Raman spectroscopy of single-wall carbon nanotubes within a polymer under strain. *Phys Rev B*, 2002, 65: 113413
- 55 Hadjiev V G, Mitchell C A, Arepalli S, et al. Thermal mismatch

- strains in sidewall functionalized carbon nanotube/polystyrene nanocomposites. *J Chem Phys*, 2005, 122: 124708
- 56 Hadjiev V G, Lagoudas D C, Oh E-S, et al. Buckling instabilities of octadecylamine functionalized carbon nanotubes embedded in epoxy. *Compos Sci Tech*, 2006, 66: 128–136
- 57 Liu L Q, Barber A H, Nuriel S, et al. Mechanical properties of functionalized single-walled carbon-nanotube/poly(vinyl alcohol) nanocomposites. *Adv Func Mater*, 2005, 15: 975–980
- 58 Zhao Q, Wood J R, Wagner H D. Using carbon nanotubes to detect polymer transitions. *J Poly Sci B*, 2001, 39: 1492–1495
- 59 Lourie O, Wagner H D. Evaluation of Young's modulus of carbon nanotubes by micro Raman spectroscopy. *J Mater Res*, 1998, 13: 2418–2422
- 60 Wagner H D. Thermal residual stress in composites with anisotropic interphases. *Phys Rev B*, 1996, 53: 5055–5058
- 61 Zhang M, Atkinson K R, Baughman R H. Multifunctional carbon nanotube yarns by downsizing an ancient technology. *Science*, 2004, 306: 1358–1361
- 62 Li Y L, Kinloch I A, Windle A H. Direct spinning of carbon nanotube fibers from chemical vapor deposition synthesis. *Science*, 2004, 304: 276–278
- 63 Xiao L, Chen Z, Feng C, et al. Flexible, stretchable, transparent carbon nanotube thin film loudspeakers. *Nano Lett*, 2008, 8: 4539–4545
- 64 Koziol K, Vilatela J, Moisala A, et al. High-Performance Carbon Nanotube Fiber. *Science*, 2007, 318: 1892–1895
- 65 Ericson L M, Fan H, Peng H Q, et al. Macroscopic, neat, single-walled carbon nanotube fibers. *science*, 2004, 305: 1447–1450
- 66 Zhang X B, Jiang K L, Chen F, et al. Spinning and processing continuous yarns from 4-inch wafer scale super-aligned carbon nanotube arrays. *Adv Mater*, 2006, 18: 1505–1510
- 67 Ma W J, Liu L Q, Yang R, et al. Monitoring a micromechanical process in macroscale carbon nanotube films and fibers. *Adv Mater*, 2009, 21: 603–608
- 68 Ma W J, Liu L Q, Zhang Z, et al. High-strength composite fibers: Realizing true potential of carbon nanotubes in polymer matrix through continuous reticulate architecture and molecular level couplings. *Nano Lett*, 2009, 9: 2855–2861
- 69 Ma W J, Song L, Yang R, et al. Directly synthesized strong, highly conducting, transparent single-walled carbon nanotube films. *Nano Lett*, 2007, 7: 2307–2311